

Differentiating the signal from the noise: towards optimal choices of wide field-of-view telescope transient follow-up

COSMIN STACHIE,¹ MICHAEL W. COUGHLIN,² NELSON CHRISTENSEN,¹ AND DANIEL MUTHUKRISHNA³

¹*Artemis, Université Côte d'Azur, Observatoire Côte d'Azur, CNRS, CS 34229, F-06304 Nice Cedex 4, France*

²*Division of Physics, Math, and Astronomy, California Institute of Technology, Pasadena, CA 91125, USA*

³*Institute of Astronomy, University of Cambridge, Madingley Road, Cambridge CB3 0HA, UK*

ABSTRACT

With the advent of the follow-up of large sky localization regions from gravitational-wave detectors and gamma-ray burst telescopes with wide field-of-view telescopes, the need for efficient follow-up of the many identified candidates is required. Due to limited telescope time, it is important to create prioritized lists of the many candidates identified. Towards this end, we use *astrorapid*, a multi-band photometric lightcurve classifier, to differentiate between kilonovae, supernovae and other possible transients. We demonstrate our method on both ideally sampled, simulated lightcurves, as well as the photometric observations of real events. We show that after only a few days of observations of an astronomical object, it is possible to rule out candidates as supernovae and other known transients.

Keywords: gravitational waves

1. INTRODUCTION

The first detection of a binary neutron star system GW170817 (Abbott et al. 2017b) by the gravitational-wave (GW) detectors Advanced LIGO and Advanced Virgo was accompanied by the detection of both a short gamma-ray burst (SGRB) by *Fermi* Gamma-Ray Burst Monitor (GBM) (Abbott et al. 2017a; Goldstein et al. 2017; Savchenko et al. 2017) and a kilonova by many other facilities (Coulter et al. 2017; Smartt et al. 2017; Abbott et al. 2017c). This *kilonova* is the ultra-violet/optical/infrared emission powered by the neutron-rich outflows undergoing the radioactive decay of r-process elements (Lattimer & Schramm 1974; Li & Paczynski 1998; Metzger et al. 2010; Kasen et al. 2017a). The specifics of the lightcurves of kilonovae depend on the equation of state (EOS) of neutron stars and the mass ratio of the binary (Bauswein et al. 2013; Piran et al. 2013; Abbott et al. 2017b; Bauswein et al. 2017; Dietrich & Ujevic 2017; Radice et al. 2018). In addition to this, there is synchrotron emission, which arises from a compact central engine launching a highly relativistic jet of electron/positron/baryon plasma (Wijers et al. 1997; Mészáros & Rees 1998). Interactions between structures within the jet produce gamma rays and hard X-rays, and the *afterglow* phase, produced by interaction of the jet with the ambient material, consists of long lasting multi-wavelength emission in the X-ray, optical, and radio. There have been a number of examples in the literature of using the photometry of both

afterglows (Troja et al. 2018) and kilonovae (Coughlin et al. 2017; Smartt et al. 2017; Coughlin et al. 2018) to place constraints on the character of the progenitor systems.

The joint observations of these systems are interesting for a variety of reasons, including the study of SGRB beaming, energetics, and galactic environment (Metzger & Berger 2012). In addition, the study of the kilonova lightcurves provides precious information about the nucleosynthesis of heavy chemical elements on the Universe (Watson et al. 2019; Drout et al. 2017; Pian et al. 2017; Kasen et al. 2017b). However the detection of the kilonova transient represents a difficult task given the large sky localizations provided by both the γ -ray satellites, such as the *Fermi* GBM and GW interferometers. The localizations released by the GW detectors, in particular, can be large, spanning $\approx 100 - 10,000$ deg² (Röver et al. 2007b; Fairhurst 2009, 2011; Grover et al. 2014; Wen & Chen 2010; Sidery et al. 2014; Singer et al. 2014; Berry et al. 2015; Essick et al. 2015; Cornish & Littenberg 2015; Klimentko et al. 2016) and also include distance information (Röver et al. 2007a; Singer et al. 2014; Berry et al. 2015; Singer et al. 2016). While GRB detections only have 2D sky localization information, the strain measurement in GW events allows also for the computation of a luminosity distance and therefore complete 3D skymap information is provided.

With the large sky localization regions that require coverage of events of this type, wide-field survey telescopes have the best opportunities to make a detection.

Observing systems such as Panoramic Survey Telescope and Rapid Response System (Pan-STARRS) (Morgan et al. 2012), Asteroid Terrestrial-impact Last Alert System (ATLAS) (Tonry et al. 2018), the Zwicky Transient Facility (ZTF) (Bellm et al. 2018; Graham et al. 2019), and in the near future BlackGEM (Bloemen et al. 2015) and the Large Synoptic Survey Telescope (LSST) (Ivezic et al. 2008), will be observing these localizations. But this advantage represents also a difficulty for the follow-up of poorly localized events given the significant number of detections per night by these surveys. In these conditions, the identification of particular transient in a large sky localization is a significant challenge. For this reason, an effective follow-up requires coordination between the wide FOV telescopes discovering transients in the localizations and the telescopes that follow-up those transients. In general, the telescopes that will follow-up and identify these transients have smaller FOV, both for photometry and spectroscopy. For this reason, it is essential to minimize the number of objects that require observations and be as efficient as possible with the available telescope time.

Techniques to optimize the follow-up of objects have been proposed in the literature. In Coughlin et al. (2019b), a method which combines the automated filtering and human vetting is used in order to reduce the number of initial candidates for S190425z (Ligo Scientific Collaboration & VIRGO Collaboration 2019), the first binary neutron star candidate from the third observing run. During the automatic analysis, asteroids or near-Earth objects are removed as they did not appear in consecutive observations separated by a few tens of minutes. Objects very close (< 2 arcsec) to point-like sources or having a historical detection prior to three days before the trigger are also automatically rejected. Finally, machine learning algorithms are used to identify image artifacts. Altogether, due to this automated filtering, it was possible to reduce the number of candidates from more than 300,000 to less than 300. Then, human vetting kept only those triggers which are in the localization, both in the 2D and distance, and which exhibited a rapid color evolution consistent with a kilonova. At the end of the entire analysis, fewer than 20 candidates remained. As another example, in Andreoni et al. (2019), one can see the importance of having data not only after the GW trigger, but also prior to it. The DECam follow-up of the GW alert S190814bvs showed that it was difficult to rule out candidates due to the lack of recent pre-imaging history, resulting in significantly more candidates despite a smaller localization to cover.

There are two kinds of objects that exhibit time variability: transients (which brighten and fade forever) and variable objects (brighten and fade periodically). Our knowledge about these electromagnetic events has dramatically improved in the last years. For some types, such as supernovae, there are models for their associated lightcurves, estimates of the rate of their occurrence, as well as the host-galaxy environment. Because of this, it is possible to simulate realistic lightcurves given a specific telescope’s sensitivity and sky background. This was performed, for example, in the LSST *PLAsTiCC* data challenge (Kessler et al. 2019). In this study, they considered both extragalactic and galactic transients. Then, by means of the SuperNova ANALYSIS software (SNANA) (Kessler et al. 2009), a realistic set of lightcurves is generated illustrating what would be the LSST detections of transients of this type in the coming years. In this paper, we will use *astrorapid* (Muthukrishna et al. 2019), a classifier tool based on machine learning to classify objects. It was trained on a set of lightcurves generated using SNANA and *PLAsTiCC* in order to simulate a realistic set of events that would be observed by ZTF. *astrorapid* is designed to distinguish between transient templates, which we will describe briefly in the following.

In this paper, we will evaluate the ability to use machine learning classifiers on early photometric lightcurves to support prioritization of transients for follow-up in GW and SGRB follow-up. While we will focus on kilonovae in this paper, the technique will be suitable for detection of afterglows. We will describe the algorithm we use in Section 2. In section 3, we describe the performance of the algorithms. In section 4, we offer concluding remarks and suggest directions for future research.

2. ALGORITHM

The idea of this analysis is to use multi-epoch photometry to identify interesting candidates. For the kilonova models being explored here, significant changes in magnitude are expected on time-scales of a single night. For this reason, telescope network photometry will determine which transients can feasibly be related to the event, and otherwise determine the background supernovae and other unrelated transients. A flow chart showing up the method used in this study (and explained further in the following) to identify and characterize optical counterparts is shown in Figure 1.

For this purpose, we use *astrorapid*, which was developed to distinguish between fourteen different templates: “Pre-explosion” (a template introduced in order to distinguish the targeted flaring event from the mo-

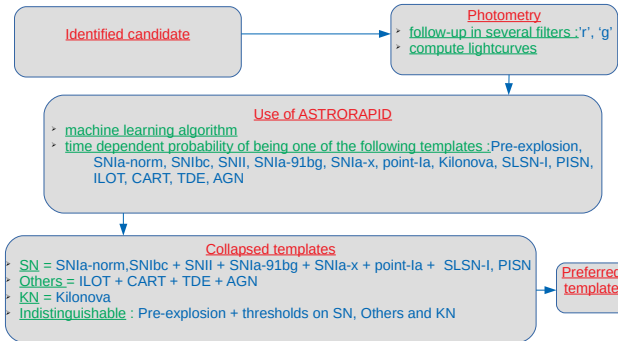


Figure 1. Flow chart illustrating the different steps made in the photometry analysis. The starting point is represented by the initial set of identified candidates, after which optical observations are carried out for each of these events. Then **astrorapid** provides a time dependent probability distribution spread over fourteen possible candidate classes. The results provided by **astrorapid** are handled in order to give weights and discriminate between only four main classes: “SN”, “KN”, “Others” and “Indistinguishable.” Finally, a preferred class is declared.

ments preceding it (Muthukrishna et al. 2019)), “SNIa-norm” (a subtype of Type Ia Supernovae), “SNIbc” (a subtype of Core collapse Supernovae), “SNII” (a subtype of Core collapse Supernovae), “SNIa-91bg” (a subtype of Type Ia Supernovae), “SNIa-x” (a subtype of Type Ia Supernovae (Silverman et al. 2012; Foley et al. 2013)), “point-Ia” (hypothetical supernova type (Shen et al. 2010)), “Kilonova” (electromagnetic counterpart to either binary neutron star (BNS) or neutron star - black hole (NS-BH) mergers (Abbott et al. 2017)), “SLSN-I” (Type I Super-luminous supernovae (Quimby et al. 2008)), “PISN” (Pair-instability Supernovae Ren et al. (2012)), “ILOT” (Intermediate Luminosity Optical Transients (Berger et al. 2009)), “CART” (Calcium-rich gap transients (Lunnan et al. 2017)), “TDE” (Tidal disruption Events (Rees 1988)), and “AGN” (Active galactic nuclei). The tool takes as input data the lightcurve of the transient, including the time of the exposure, apparent magnitude and associated error bar; the output consists of a time-dependent discrete probability distribution. It can take either a redshift (such as from a probable host galaxy) or not, and we will show results for both cases in the following. This distribution provides the probability for each one of the 14 template types. The probability distribution changes with every new observation, and the more points the lightcurve contains, the more precise the identification.

While **astrorapid** was designed to classify full lightcurves, the goal of this analysis is to determine, given a few observations, how to prioritize objects for follow-up to support kilonova identification. To

this end, we made a few modifications to the initial code. First of all, we collapse all fourteen different templates into three main classes. Thus we consider the following classes: “SN” (which accounts for “SNIa-norm,” “SNIbc,” “SNIa-91bg,” “SNIa-x,” “point-Ia,” “SLSN-I,” “PISN”), “Others” (accounting for “ILOT,” “CART,” “TDE,” and “AGN”) and “KN” (which is simply the “Kilonova” template). The probability of “Others” and “KN” is simply the sum of the probabilities of their constituents. For the new probability for the “SN” class in particular, we found that we required to penalize it more than the others (likely because it is made up of a majority of the classes); therefore, for “SN” in particular, we use the sum of the probabilities of its components multiplied by the factor $(1 - e^{-k_{\text{obs}}^{\text{th}} * 0.25})$, where $k_{\text{obs}}^{\text{th}}$ stands for the $(k + 1)^{\text{th}}$ observation. The multiplication factor $(1 - e^{-k_{\text{obs}}^{\text{th}} * 0.25})$ is motivated by the fact that the “SN” class accounts for numerous **astrorapid** templates and so even negligible once summed, it generates a large probability for the very first observations. We found this penalty factor by hand in order to make accurate classifications at early times. Then, we also introduce a new class called “Indistinguishable”, where we will say that the preferred event is “Indistinguishable” if none of the other classes (“SN,” “KN,” and “Others”) has a probability higher than 40%. The 40% threshold was selected at the end of several trials. This value represents a trade off between two different behaviors. A higher threshold will favor too much the “Indistinguishable” class at least for the very first observations where there is not much information and the initial weight of the “Pre-explosion” template is already high. On the other hand, the consequence of a lower threshold will be to force the modified classifier to choose some class in {“SN”, “KN”, “Others”}, although there is not enough information for any inference; this is also an undesirable effect. In summary, in total there are 4 classes: “KN,” “SN,” “Others” and “Indistinguishable.” We also now introduce the idea of a “preferred event” after n observations. We define the preferred event as X (here X stands for “KN”, “SN” or “Others”) if two conditions are fulfilled: (i) $Prob(X) = \max(Prob(\text{“SN”}), Prob(\text{“KN”}), Prob(\text{“Others”}))$ and (ii) $Prob(X) > 40\%$. This will be convenient for classification later.

3. PERFORMANCE

To demonstrate the utility of the method for transient prioritization and identification, we seek to show that two conditions hold. The first is that kilonova lightcurves should in general be identified in the “KN” class. The second is that for input lightcurves represent-

ing some other transient type, the analysis should not misidentify it as a “KN.” In the following, we will use both simulated lightcurves and real ZTF astrophysical transients from the public survey to assess these questions. For the injection sets in particular, we will create two sets of simulated SNe and KNe lightcurves. Each set has 1,000 lightcurves representing transients uniformly distributed in distance between 40 Mpc and 3,000 Mpc. The set of real ZTF events is formed by 2,291 lightcurves from the public data stream with an average of 29 observations per lightcurve. These events are mainly different types of supernovae, but also include transients like TDE, AGN, ILOT and CART.

3.1. Injection sets

As described above, we use simulations of both kilonova and supernova lightcurves generated by varying different parameters. The codebase used to generate kilonova lightcurves was described previously in Coughlin et al. (2018b) and Coughlin et al. (2018a). The variable physical parameters in the model are the ejecta mass (M_{ej}), the velocity of the ejecta (v_{ej}) and the lanthanide fraction (X_{lan}). Likewise, the prior range of the parameters are $M_{ej} \in [0.01M_{\odot}, 0.1M_{\odot}]$, $v_{ej} \in [0.01c, 0.3c]$ and $X_{lan} \in [10^{-5}, 10^{-1}]$, where M_{\odot} is the solar mass and c represents the light velocity. While v_{ej} is sampled uniformly, the parameters X_{lan} and M_{ej} are log-uniformly distributed. An illustration of several such lightcurves is given on the right of Figure 2. Type Ia supernovae lightcurves are generated by “sncosmo,” whose details are explained in Barbary et al. (2016); Guy et al. (2007). In order to be as general as possible, parameters like parameter shape (hereafter x_1) and color index (hereafter c) were chosen to fill a broad space: $x_1 \in [-0.5, 0.5]$ and $c \in [-0.05, 0.05]$. The left of figure 2 shows a few such lightcurves. To best imitate the “background” introduced by such lightcurves in searches for kilonovae, only the observational points corresponding to ± 7 days around the peak of the lightcurve were injected. Concerning the distance, we considered a uniformly distributed population of supernovae and kilonovae between 40 Mpc and 300 Mpc (chosen as the edge of the gravitational-wave detector horizons). Both sets of lightcurves are well-sampled (2 observations per night on average) and detections in two filters (r-band and g-band).

3.2. Injection set recoveries

We now check the performance of our method on the simulated lightcurves. While in the case of kilonova injections, the output assesses how well the classifier recognizes a kilonova; the purpose of evaluating the output

on supernovae injections is to quantify how often our tool misidentifies a transient as being a kilonova when it is not. In this regard, the supernova transients represent our “background.” The choice of supernovae as this background set is motivated by the dominance of this type of transient among the identified candidates.

We start by testing our followup on kilonova lightcurves. In Figure 3, there is the histogram of preferred events for the very first night of observations. As expected, the category “Indistinguishable” is favored when there is not enough observations (usually less than ~ 6), but at the end of two nights, the classifier identifies it as a kilonova lightcurve with a high probability. From Figure 3, two conclusions can be made. First, one can see that after only two days of observations, the “KN” template starts to be preferred over the others. Second, one notices that after 3 days of observations, the classifier mainly chooses the “KN” template, and the few failures consist of preference for the “SN” and “Indistinguishable” templates. The false alarm rate is less than 4 per 10 events. In Figure 4 shows the dependence of the classifier’s preferred events (at the end of 3 days of observation) as a function of X_{lan} , redshift, M_{ej} and v_{ej} .

Figure 4 suggests that the velocity of the ejecta does not significantly change the lightcurve from the classifier’s point of view, while the more mass ejected leads to a higher preference for the “SN” templates; this is because they become brighter and therefore more consistent with supernovae. It also reveals that the lanthanide fraction and the redshift have a non-negligible impact on the lightcurve; we see that the smaller X_{lan} , the more probable is the “SN” template, and the higher X_{lan} , the more probable is “Indistinguishable.” The lanthanide fraction is responsible for the reddening of the lightcurve. As the lanthanide fraction decreases, the transient becomes more blue and therefore compatible with a supernova lightcurve (which are in general more gray). In addition, a large lanthanide fraction leads to red lightcurves, where the g-band observations are upperlimits instead of detections and so the “Indistinguishable” template becomes the favored one, as there is no color information. For the redshift, for higher values of redshift, the absolute magnitudes are lower (for a fixed apparent magnitude). Therefore, a small value of the redshift means an intrinsically brighter transient event and thus more likely a supernova. On the other hand, a high value of the redshift denotes a small signal to noise ratio, and thus the classifier is also more likely to prefer the “Indistinguishable” template. In the case of the supernova injections (see Figure 5), the “SN” template is preferred after only a few nights. This is because these

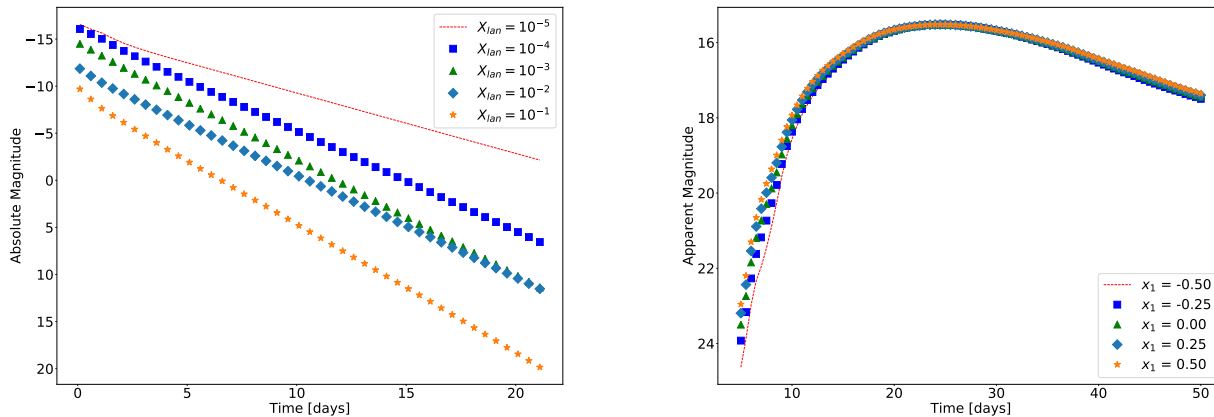


Figure 2. Left: Lightcurves representing the Absolute Magnitude as a function of time for five KN injections, for different input parameters. For all the lightcurves $M_{ej} = 0.05M_{\odot}$ and $v_{ej} = 0.15c$. The only parameter that varies is X_{lan} , whose value is shown on the legend. Right: Apparent Magnitude versus time for five SN injections. The lightcurves share parameters like cosmological redshift $z = 0.22$ and color index $c = 0$. Instead the shape parameter x_1 is different for each lightcurves and its value is shown in the legend. For both plots, these are the simulation results for the g-band.

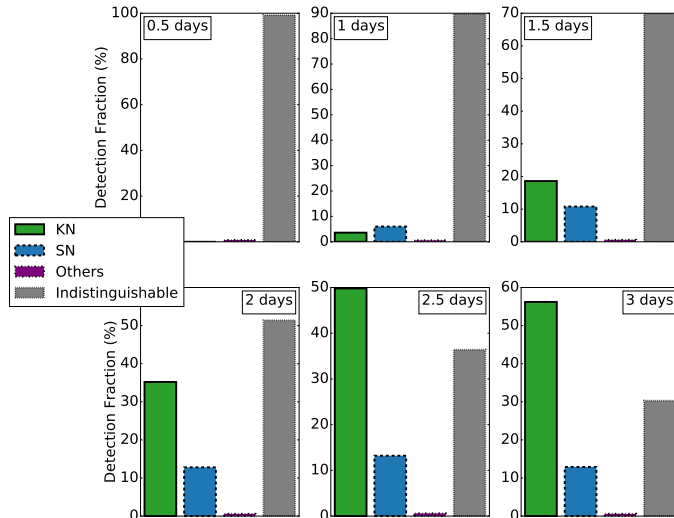


Figure 3. Preferred event fraction histogram given different amounts of observation time: from 0.5 days (top-left corner) up to 3 days (bottom-right corner). The input is represented by the set of 1000 kilonovae injections.

are the brightest transient events, and therefore their brightness is the key determinant.

3.3. Real transients observed in multiple filters

In the case of injections, we considered only ideally sampled lightcurves; the study of realistically sampled lightcurves is necessary to assess the performances of our classifier in realistic situations. To this end, we use public ZTF lightcurves. Like before, we put these events in two categories: “SN” and “Other.” There are 2,049 “SN” type events (1450 “SNIa,” 110 “SNIbc,” 447 “SNIi,” and 42 “SLSN”) and 174 “Others” type events

(152 “AGN,” 4 “CART,” 6 “ILOT,” and 12 “TDE”). In Figure 6, one can see the results of the classifier after the first observation points in the case of “SN” and “Others” type real events. One can see that the classifier starts to behaves well after only 11 observations in the identification of “SN” and 16 in the “Others” case. It also shows that the classifier almost never misidentifies these real events as being kilonovae.

3.4. Real transients observed in a single filter

Among the real supernovae transient lightcurves, events there are 157 transients which have only single passband observations. As for any deep learning algorithm, the idea is that the more information there is, the better is the classification. Therefore, it is worthwhile a comparison of the performances of the classifier between the situation where there are two filters to the situation in which only one passband is available. In Figure 7, we show the results of the follow-up on those single filter events. In this case, the success rate after 26 observations is much lower (around 10%) compared to the case presented in the previous section (success rate around 60%). This highlights how essential color information is in the classification. It is worth mentioning that SNANA (Kessler et al. 2009) sims that *astrophorapid* was trained on did not include single filter light curves, therefore retraining *astrophorapid* to include both single and multi photometric bands will help to fix this issue in future.

3.5. The redshift as a supplementary information

In the previous sections, we presented the results of our method when the input consists only of photometric

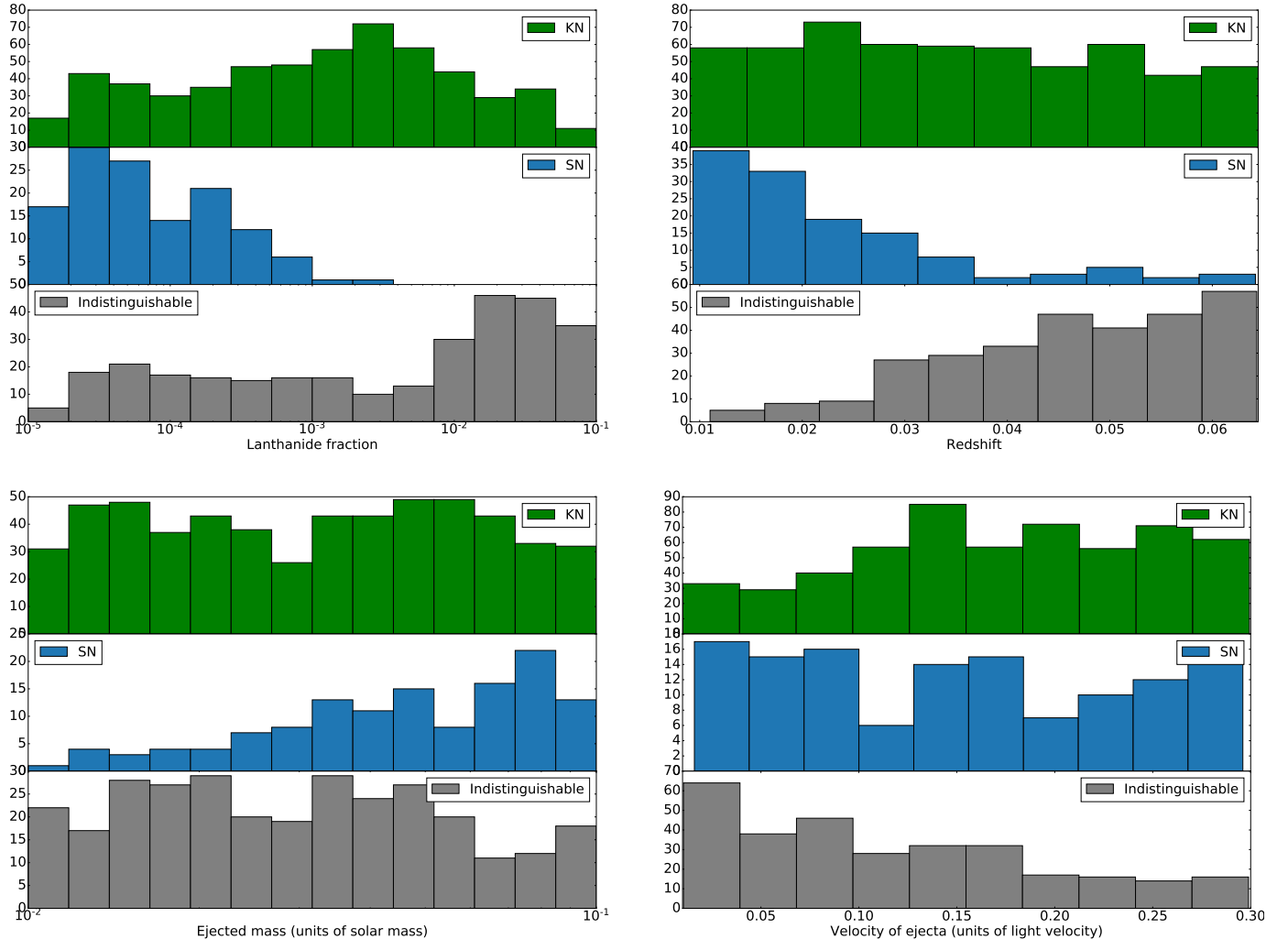


Figure 4. Classifications results dependence on the varied parameters for the 1000 KN injections. On the top row, a histogram of classifier’s favored events after 3 days of observation as a function of X_{lan} (on the left) and redshift (on the right). On the bottom row is the same as a function of M_{ej} (on the left) and v_{ej} (on the right)

data. But as any classifier based on machine learning, **astrorapid** provides more precise classifications if additional information is available. One example of such additional information might be the redshift of the candidate. In Figure 8, it is illustrated by means of a histogram the quantitative improvement in the classification results when the redshift is known compared to the situation where this information is unknown. One can observe that at the end of two nights of observations the success rate in the recovery of KN templates is improved by more than 10% if the cosmological redshift is given.

4. CONCLUSION

In this study, we presented a method to classify transients starting from photometric observations and the cosmological redshift. The method is based on the use of an open-source classifier **astrorapid**. By running

this tool on input data represented by the observational lightcurves and combining the output results by source class, we propose a way to distinguish between four main classes: “KN”, “SN”, “Others” and “Indistinguishable.” The performance of this classifier and class system have been tested on both simulated lightcurves and real ZTF objects. In the case of ideally sampled lightcurves, it has been shown that the identification of SNe necessitates only a few observations in multiple passbands, while for the recognition of KNe, a few nights of photometry in multiple passbands is required (with significantly worse results in the case of single passband observations). Finally, the set of real transients from the public ZTF alert stream emphasizes the necessity of around 10 observations at the ZTF cadence.

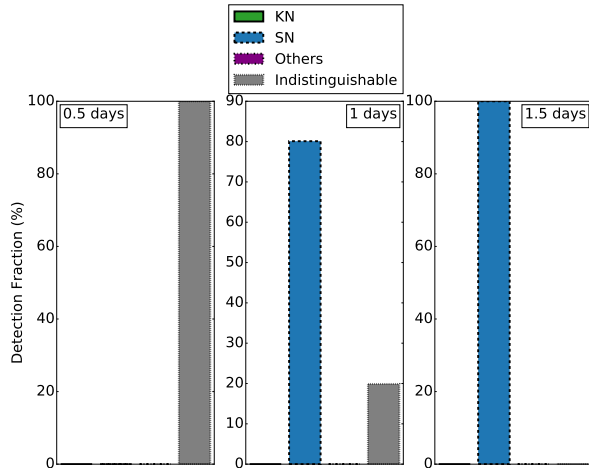


Figure 5. Preferred event fraction histogram given different amounts of observation time: from 0.5 days (left) up to 1.5 days (right). The input is represented by the set of 1000 SN injections.

In the future, we intend to improve `astrorapid` to account for “missing” observations where only upperlimits are available. This should be useful in cases of particularly red or blue transients, where likely the color information is even *more* apparent than in the case where there are detections. In addition, we plan to incorporate this technique into some of the ongoing follow-up infrastructure, such as the GROWTH target of opportunity marshal (Coughlin et al. 2019a) and the GRANDMA iCARE pipeline (Antier et al. 2019).

5. ACKNOWLEDGMENTS

MC is supported by the David and Ellen Lee Prize Postdoctoral Fellowship at the California Institute of Technology. The authors thank the Observatoire de la Côte d’Azur for support.

REFERENCES

- Abbott, B. P., Abbott, R., Abbott, T. D., et al. 2017, *Phys. Rev. Lett.*, 119, 161101
- Abbott et al. 2017a, *The Astrophysical Journal Letters*, 848, L13
- . 2017b, *Phys. Rev. Lett.*, 119, 161101
- . 2017c, *The Astrophysical Journal Letters*, 848, L12
- Andreoni, I., et al. 2019, arXiv:1910.13409
- Antier, S., et al. 2019, arXiv:1910.11261
- Barbary, K., Barclay, T., Biswas, R., et al. 2016, *Astrophysics Source Code Library*
- Bauswein, A., Baumgarte, T. W., & Janka, H.-T. 2013, *Phys. Rev. Lett.*, 111, 131101
- Bauswein et al. 2017, *The Astrophysical Journal Letters*, 850, L34
- Bellm, E. C., Kulkarni, S. R., Graham, M. J., et al. 2018, *Publications of the Astronomical Society of the Pacific*, 131, 018002
- Berger, E., Soderberg, A., Chevalier, R., et al. 2009, *The Astrophysical Journal*, 699, 1850
- Berry, C. P. L., Mandel, I., Middleton, H., et al. 2015, *Astrophys. J.*, 804, 114
- Bloemen, S., Groot, P., Nelemans, G., & Klein-Wolt, M. 2015, in *Astronomical Society of the Pacific Conference Series*, Vol. 496, *Living Together: Planets, Host Stars and Binaries*, ed. S. M. Rucinski, G. Torres, & M. Zejda, 254
- Cornish, N. J., & Littenberg, T. B. 2015, *Classical and Quantum Gravity*, 32, 135012
- Coughlin, M., Dietrich, T., Kawaguchi, K., et al. 2017, *ArXiv e-prints*, arXiv:1708.07714
- Coughlin, M. W., Dietrich, T., Doctor, Z., et al. 2018, *ArXiv e-prints*, arXiv:1805.09371
- Coughlin, M. W., Ahumada, T., Cenko, S. B., et al. 2019a, *Publications of the Astronomical Society of the Pacific*, 131, 048001
- Coughlin, M. W., et al. 2019b, *Astrophys. J.*, 885, L19
- Coughlin et al. 2018a, *Mon. Not. Roy. Astron. Soc.*, 480, 3871
- . 2018b, arXiv:1812.04803
- Coulter et al. 2017, *Science*, 358, 1556
- Dietrich, T., & Ujevic, M. 2017, *Class. Quant. Grav.*, 34, 105014
- Drout, M. R., Piro, A. L., Shappee, B. J., et al. 2017, *Science*, 358, 1570
- Essick, R., Vitale, S., Katsavounidis, E., Vedovato, G., & Klimentenko, S. 2015, *The Astrophysical Journal*, 800, 81
- Fairhurst, S. 2009, *New J. Phys.*, 11, 123006
- Fairhurst, S. 2011, *Class. Quant. Grav.*, 28, 105021
- Foley, R. J., Challis, P. J., Chornock, R., et al. 2013, *The Astrophysical Journal*, 767, 57
- Goldstein et al. 2017, *The Astrophysical Journal Letters*, 848, L14
- Graham, M. J., Kulkarni, S. R., Bellm, E. C., et al. 2019, *Publications of the Astronomical Society of the Pacific*, 131, 078001

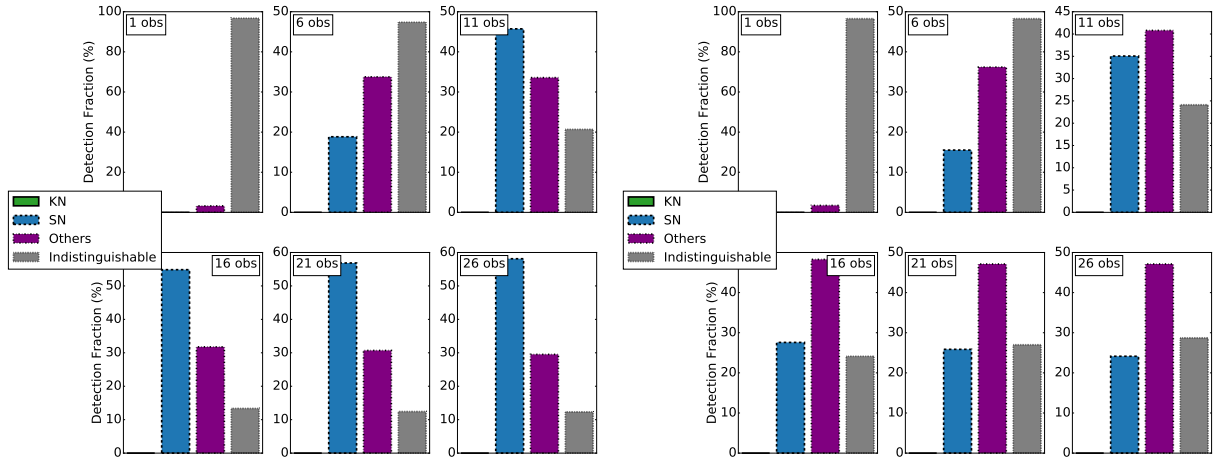


Figure 6. On the left is the histogram of classifier favored events given different number of observations: from 1 (top-left corner) up to 26 (bottom-right corner). The input is represented by the set of 2,049 ZTF real sources identified as “SN” type. On the right is the same for the set of 174 ZTF real sources identified as the “Others” type.

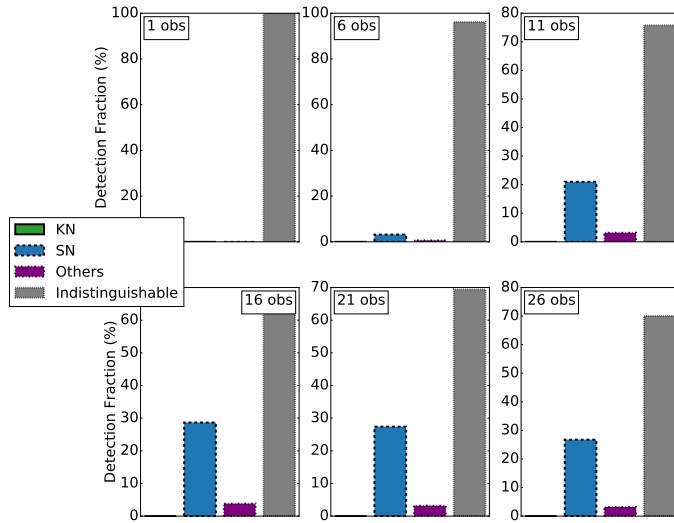


Figure 7. Preferred template fraction for after different number of observations: from 1 (top-left corner) up to 26 (bottom-right corner). The input is represented by the set of 157 ZTF real sources observed in only one filter. Those events were finally all identified as being SN types.

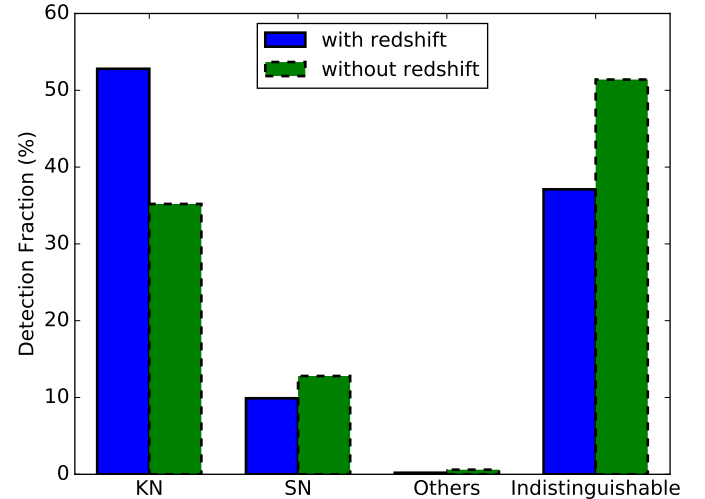


Figure 8. Classifications results after 2 nights of observations with (blue) and without (green) the knowledge of the cosmological redshift. The input is represented by the same 1000 “KN” injections set discussed in the previous subsections.

Grover, K., Fairhurst, S., Farr, B. F., et al. 2014, Phys.

Rev., D89, 042004

Guy, J., et al. 2007, Astron. Astrophys., 466, 11

Ivezic, Z., Tyson, J. A., Allsman, R., Andrew, J., & Angel, R. 2008, arXiv:0805.2366

Kasen, D., Metzger, B., Barnes, J., Quataert, E., & Ramirez-Ruiz, E. 2017a, Nature, 551, 80 EP

—. 2017b, Nature, arXiv:1710.05463, [Nature551,80(2017)]

Kessler, R., Bernstein, J. P., Cinabro, D., et al. 2009, Publications of the Astronomical Society of the Pacific, 121, 1028

Kessler, R., et al. 2019, Publ. Astron. Soc. Pac., 131, 094501

Klimenko, S., Vedovato, G., Drago, M., et al. 2016, Phys.

Rev. D, 93, 042004

Lattimer, J. M., & Schramm, D. N. 1974, ApJL, 192, L145

Li, L.-X., & Paczynski, B. 1998, The Astrophysical Journal Letters, 507, L59

Ligo Scientific Collaboration, & VIRGO Collaboration. 2019, GRB Coordinates Network, 24168, 1

Lunnan, R., Kasliwal, M. M., Cao, Y., et al. 2017, The Astrophysical Journal, 836, 60

Mészáros, P., & Rees, M. J. 1998, The Astrophysical Journal Letters, 502, L105

- Metzger, B. D., & Berger, E. 2012, *Astrophys. J.*, 746, 48
- Metzger, B. D., Martínez-Pinedo, G., Darbha, S., et al. 2010, *Monthly Notices of the Royal Astronomical Society*, 406, 2650
- Morgan, J. S., Kaiser, N., Moreau, V., Anderson, D., & Burgett, W. 2012, *Proc. SPIE Int. Soc. Opt. Eng.*, 8444, 0H
- Muthukrishna, D., Narayan, G., Mandel, K. S., Biswas, R., & Hloek, R. 2019, *Publ. Astron. Soc. Pac.*, 131, 118002
- Pian, E., et al. 2017, *Nature*, 551, 67
- Piran, T., Nakar, E., & Rosswog, S. 2013, *Monthly Notices of the Royal Astronomical Society*, 430, 2121
- Quimby, R., Aldering, G., Wheeler, J., et al. 2008, *The Astrophysical Journal Letters*, 668, L99
- Radice et al. 2018, *The Astrophysical Journal Letters*, 852, L29
- Rees, M. J. 1988, *Nature*, 333, 523
- Ren, J., Christlieb, N., & Zhao, G. 2012, *Research in Astronomy and Astrophysics*, 12, 1637
- Röver, C., Meyer, R., & Christensen, N. 2007a, *Phys. Rev. D*, 75, 062004
- Röver, C., Meyer, R., Guidi, G. M., Viceré, A., & Christensen, N. 2007b, *Classical and Quantum Gravity*, 24, S607
- Savchenko, V., Ferrigno, C., Kuulkers, E., et al. 2017, *The Astrophysical Journal Letters*, 848, L15
- Shen, K. J., Kasen, D., Weinberg, N. N., Bildsten, L., & Scannapieco, E. 2010, *Thermonuclear Ia Supernovae from Helium Shell Detonations: Explosion Models and Observables*, , arXiv:1002.2258
- Sidery, T., Aylott, B., Christensen, N., et al. 2014, *Phys. Rev.*, D89, 084060
- Silverman, J. M., Foley, R. J., Filippenko, A. V., et al. 2012, *Monthly Notices of the Royal Astronomical Society*, 425, doi:10.1111/j.1365-2966.2012.21270.x
- Singer, L. P., Price, L. R., Farr, B., et al. 2014, *Astrophys. J.*, 795, 105
- Singer et al. 2016, *The Astrophysical Journal Letters*, 829, L15
- Smartt et al. 2017, *Nature*, 551, 75 EP
- Tonry, J. L., Denneau, L., Heinze, A. N., et al. 2018, *Publications of the Astronomical Society of the Pacific*, 130, 064505
- Troja, E., Piro, L., Ryan, G., et al. 2018, *Monthly Notices of the Royal Astronomical Society*, arXiv:1801.06516
- Watson, D., et al. 2019, *Nature*, 574, 497
- Wen, L., & Chen, Y. 2010, *Phys. Rev.*, D81, 082001
- Wijers, R. A. M. J., Rees, M. J., & Mszros, P. 1997, *Monthly Notices of the Royal Astronomical Society*, 288, L51